Recent Advances in Fiber Lasers for Nonlinear Microscopy

Article *in* Nature Photonics · November 2013

DOI: 10.1038/nphoton.2013.284 · Source: PubMed

2 authors:

Chris Xu
Cornell University
403 PUBLICATIONS **20,697** CITATIONS
SEE PROFILE

Frank W Wise
Cornell University
650 PUBLICATIONS **37,008** CITATIONS
SEE PROFILE

nature photonics

FOCUS | REVIEW ARTICLES

PUBLISHED ONLINE: 20 OCTOBER 2013 | DOI: 10.1038/NPHOTON.2013.284

Recent advances in fibre lasers for nonlinear microscopy

C. Xu and F. W. Wise

Nonlinear microscopy techniques developed over the past two decades have provided dramatic new capabilities for biological imaging. The initial demonstrations of nonlinear microscopies coincided with the development of solid-state femtosecond lasers, which continue to be the dominant light source for applications of nonlinear microscopy. Fibre lasers offer attractive features for biological and biomedical imaging, and recent advances are promising for the development of high-performance sources with the potential for realizing integrated instruments that are robust and inexpensive. This Review discusses recent advances, and identifies challenges and opportunities for fibre lasers in nonlinear bioimaging.

Optical microscopy offers well-established techniques for imaging with submicrometre spatial resolution. In the past two decades, researchers have found that ultrashort light pulses can be exploited in a variety of new biomedical imaging modalities. Several techniques exploit the high peak powers achievable with ultrashort pulses, by focusing the pulses to high intensities to drive nonlinear optical processes such as multiphoton absorption in molecules used as fluorescent labels.

Since its initial demonstration in 1990[1], two-photon microscopy (2PM) has been increasingly applied to cell biology and neuroscience[2–5]. The field has been significantly broadened by several variations of 2PM, including three-photon microscopy (3PM)[6–8], second- and third-harmonic generation imaging[9–12], near-field enhanced multiphoton excitation[13], multiphoton endoscopic imaging[14] and super-resolution imaging using stimulated-emission depletion[15]. The development of various fluorescent indicators, particularly genetically engineered probes based on fluorescent proteins[16], has further enhanced the capabilities of multiphoton microscopy (MPM). The current state of microscope technology is summarized in ref. 17. Efficient multiphoton excitation requires peak intensities in the range 0.1–1 TW. In addition to tight spatial focusing, MPM typically requires pulsed excitation sources so that efficient excitation can be obtained at a practical average power. For example, a femtosecond laser with a pulse duration (τ) of 100 fs at a pulse repetition rate (f) of 100 MHz will enhance the two-photon excitation probability relative to that for continuous-wave light by the inverse of the duty cycle ($f \times \tau$), which is a factor of approximately 10^5.

Multiphoton and harmonic-generation microscopies are based on electronic transitions. A number of biologically important substances (for example, lipids, nucleic acids and sugars) have characteristic vibrational spectra, which allows them to be distinguished easily. The combination of microscopy with vibrational spectroscopy thus permits images with chemical contrast to be generated; this is the basis of coherent Raman scattering (CRS) microscopies. Coherent anti-Stokes Raman scattering (CARS) microscopy is a sensitive nonlinear technique that offers chemical selectivity[18,19] without the use of exogenous dyes. The CARS signal is complicated by the presence of an electronic contribution; stimulated Raman scattering microscopy[20,21] was mainly developed to isolate the vibrational response.

A dye laser supplied the femtosecond pulses for the first multiphoton fluorescence images[1], but dye lasers have low output powers and require expert operators. The discovery of Kerr-lens mode locking in titanium-doped sapphire lasers[22,23] was critical to the proliferation of nonlinear microscopy. Commercial Ti:sapphire lasers became available in the early 1990s. Other solid-state laser media, such as Nd:glass[24], Yb:glass[25], Yb:tungstate[26] and Cr:forsterite[27], have also been developed. These sources have enabled the dramatic growth of multiphoton and harmonic-generation imaging. Standard Ti:sapphire lasers are tunable in the range 700–1,000 nm, with pulse energies in the range 20–30 nJ, pulse durations under 100 fs, repetition rates around 100 MHz and average powers of 2 W. Existing solid-state lasers are outstanding laboratory tools. At least one commercial instrument (InSight™ DeepSee™ Ultrafast Laser, Newport Spectra-Physics) covers the remarkably wide range of 680–1,300 nm. The infrastructure to support 2PM within this spectral window is well established. However, stable, user-friendly instruments that are less expensive and more compact should allow multiphoton fluorescence microscopy to find application in a range of new settings. The development of appropriate short-pulse sources will also facilitate the expansion of CRS microscopies. The continued demonstration of new microscopy techniques further motivates the development of appropriate short-pulse sources.

Advances in high-energy, femtosecond fibre oscillators

Fibre lasers are attractive for imaging applications for the following reasons: (i) the waveguide medium of fibre lasers largely eliminates the need for precise optical alignment, enables long cavities (and hence low repetition rates) and ensures good beam quality; (ii) fibre gain media are efficient and can easily supply the power needed for bioimaging; (iii) fibre lasers are naturally suitable for integration with endoscopic instruments.

Short-pulse fibre lasers have attracted substantial research attention, and progress has been reviewed in a number of papers[28–31]. However, the performance of fibre lasers has historically lagged behind that of solid-state lasers. Amplifier systems have sometimes been required, increasing the complexity and cost. In addition, fibre lasers are not broadly wavelength tunable. As a result, solid-state lasers still dominate the field of nonlinear microscopy.

Recently demonstrated femtosecond fibre lasers can match, and even exceed, the performance of solid-state lasers, albeit at one wavelength. Work is thus needed to extend their wavelength range, although their present power levels will allow efficient frequency conversion to new wavelengths. Thus, short-pulse fibre sources will continue to improve, and offer new alternatives to existing solid-state

School of Applied and Engineering Physics, Cornell University, Ithaca, New York 14853, USA. *e-mail: chris.xu@cornell.edu; frank.wise@cornell.edu

NATURE PHOTONICS DOI: 10.1038/NPHOTON.2013.284

lasers in many nonlinear bioimaging applications. Although this will have a substantial impact, we believe that fibre lasers are potentially capable of much more than simply matching existing capabilities — fibre lasers offer design flexibility that will allow the creation of new combinations of performance parameters, which can be customized to specific bioimaging applications.

Since the first demonstrations of reliable instruments in the 1980s[32], femtosecond lasers have been based on cavities with anomalous-dispersion segments. Soliton pulses form by the balance of nonlinear refraction and anomalous dispersion. The soliton energy in a fibre laser is 10–100 times lower than that in a solid-state laser, which highlights the challenge that arises in the design of fibre lasers for photophysical applications. The first step in increasing the peak power of fibre lasers was the demonstration of lasers with segments of normal and anomalous dispersion with nearly equal magnitudes. The resulting 'breathing' of the pulse temporal profile reduces the intracavity peak power, and disrupts the resonant production of dispersive waves that occurs with ordinary solitons and ultimately limits their energy. Femtosecond fibre lasers based on this 'stretched-pulse' technique[33,34] have reached nanojoule energies and 10-kW power levels.

The demonstration of femtosecond fibre lasers without any anomalous-dispersion components[35] countered two decades of accumulated understanding of short-pulse generation. In these lasers, pulses are formed by balancing the nonlinear gain and loss as well as nonlinear refraction and dispersion. They are called dissipative solitons because dissipative processes, such as nonlinear gain and loss, play a key role in their formation[36–38]. The important point for applications is that dissipative solitons can be stable at energies at least an order of magnitude larger than ordinary or dispersion-managed solitons. This is partly because dissipative solitons are chirped to 10–100 times the transform-limited duration throughout the laser cavity so that the pulse does not breathe much. Intuitively, pulse shaping is the result of filtering the chirped pulse: cutting the edges of the spectrum corresponds to cutting the leading and trailing wings of the pulse in time.

A dissipative-soliton laser was the first fibre laser to reach the power of a standard Ti:sapphire laser[39]. This laser (Fig. 1) consists mostly of Yb-doped gain fibre. The filter dominates the steady-state pulse shaping. The wave plates and polarizing beam splitter function as a saturable absorber through nonlinear polarization rotation, which is needed to start the mode locking from noise. The laser generates 20-nJ and 80-fs pulses (Fig. 1) after dechirping. Chichkov *et al.* reported further scaling of dissipative-soliton lasers to 80-nJ and 30-fs pulses[40]. The 'cat-ear' spectrum is a characteristic of dissipative-soliton lasers, and its steep sides imply some secondary structure in the time-domain pulse (Fig. 1). For the nonresonant processes exploited in nonlinear microscopy, the pedestals have little consequence beyond reducing the peak power by ~10% compared to a Gaussian pulse. For applications that place a premium on temporal pulse contrast, it is possible to take the output of a dissipative-soliton laser after the filter[41]. This produces a smoother spectrum and a cleaner pulse, albeit with some sacrifice in pulse energy. A normal-dispersion laser based on self-similar pulse evolution in the gain segment would be an alternative approach to high-energy pulses with clean profiles[42].

The high peak power and 1,050-nm wavelength of Yb-based dissipative soliton lasers are attractive for nonlinear microscopy. As an early example, images were obtained of neurons and vasculature at depths of nearly 1 mm in the cortex of a living mouse[43,44] (Fig. 2). A similar laser was integrated with a delivery fibre and a hand-held probe to produce a compact, portable system capable of producing 2PM and second-harmonic images[45].

The stable pulse energy in a laser is determined primarily by the nonlinear phase accumulated by the pulse, so it scales with the mode-field area. Fibres with larger mode areas[29,46] can be used to enhance lasers based on any pulse evolution. Lefrancois *et al.* reported a dissipative-soliton laser in which an Yb-doped photonic-crystal fibre (PCF) with a 40-μm core diameter was used in place of an ordinary gain fibre[47]. The laser generated 100-nJ and 100-fs pulses with a peak power of 1 MW and an average power of 8 W. By using a photonic-crystal rod with an even larger mode area, Baumgartl *et al.* achieved 850-nJ pulses with a peak power of 6 MW and an average power of over 60 W from a dissipative-soliton laser[48]. These remarkable performance levels currently require sacrificing some of the benefits of standard fibres, but they highlight the potential of mode-locked fibre lasers. Another possible approach for increasing the mode-field area is based on higher-order-mode (HOM) fibres[49], which retain the mechanical flexibility of large-mode-area fibres. However, two mode conversions are required to achieve HOM propagation and then return to the fundamental mode. HOM fibres with similar mode-field areas as photonic-crystal rods have been demonstrated[50].

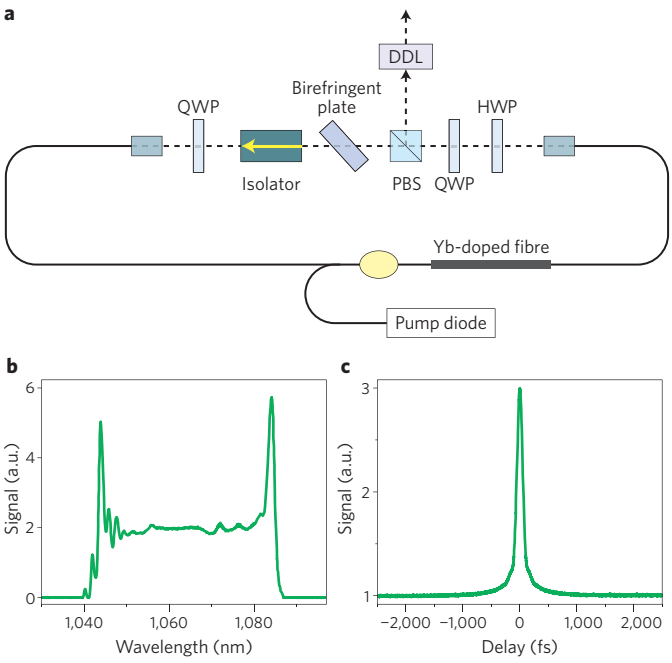

Figure 1 | Dissipative soliton laser and pulses. a, Schematic of dissipative-soliton laser cavity. QWP, quarter-wave plate; HWP, half-wave plate; PBS, polarizing beam splitter; DDL, dispersive delay line. **b**,**c**, Spectrum (**b**) and autocorrelation (**c**) of 80-fs pulse from a dissipative-soliton laser. Figure reproduced with permission from ref. 39, © 2009 OSA.

Emerging trends in multiphoton microscopy

Tissue generally scatters light effectively, making it challenging to image structures lying deep within tissue. Optical imaging has been limited to thin (typically ~0.5 mm) samples or superficial tissue. Non-invasive imaging techniques that deliver submicrometre spatial resolutions and millimetre tissue penetration depths will have a major impact on bioimaging. Applications that require imaging deep in scattering tissues[5], particularly *in vivo*, showcase the unique advantages of MPM. 2PM has been successfully applied to a variety of deep-tissue imaging applications, including direct visualization of neuronal activity[51] and anatomy[52], developing embryos[53], and tissue morphology and pathology[54,55]. 2PM offers penetration depths that are two to three greater than those of linear confocal microscopy[56].

The imaging depth for high-resolution 2PM is limited by the signal-to-background ratio of the fluorescence distribution in

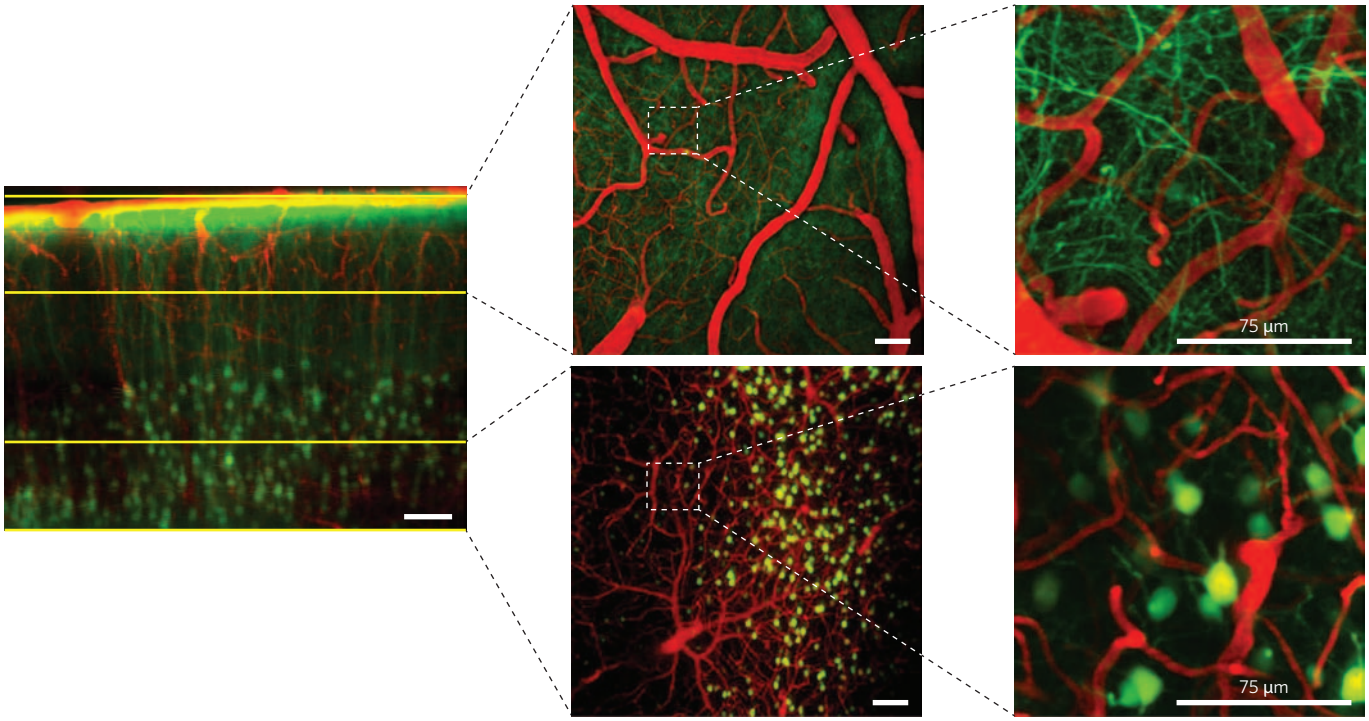

Figure 2 | Two-photon fluorescence images obtained using excitation from a dissipative-soliton fibre laser. Images of the cortex of a live, anaesthetized mouse with a glass-covered craniotomy, recorded in the laboratory of C. Schaffer at Cornell University. Pyramidal neurons are labelled by yellow fluorescent protein (green) and blood vessels are labelled by intravenously injected Texas Red dextran (red). The top row shows surface vessels and dendritic processes in the top 150 μm; the bottom row shows arterioles, venules, capillaries and neuron cell bodies at depths of 450–650 μm. Yellow boxes (left) delineate areas of higher magnification (right). Figure reproduced with permission from ref. 43, © 2012 IEEE.

scattering tissue[57]. This depth limit for 2PM is approximately five to six effective attenuation lengths (l_e)[58,59] (for example, ~700 μm in the mouse neocortex with 775-nm excitation). Using longer excitation wavelengths reduces the impact of tissue scattering[60–62], but there is a trade-off between tissue scattering and absorption. This trade-off defines the optimum excitation wavelength for tissue penetration. Figure 3 shows the water absorption length (l_a) and the calculated scattering length (l_s) of mouse brain tissue. The combined effect of absorption and scattering is expressed by $l_e = (1/l_a + 1/l_s)^{-1}$ (ref. 63). The validity of Fig. 3 for brain imaging is confirmed by previous measurements of the effective attenuation coefficient (indicated by the yellow circles). Figure 3 clearly indicates that the optimum wavelength windows for deep-tissue imaging are near 1,300 nm and 1,700 nm.

With longer-wavelength excitation, particularly ~1,700 nm, many endogenous fluorophores (for example, NADH) become inaccessible, even by three-photon excitation (3PE). Although this may limit clinical applications involving human subjects, longer excitation wavelengths are beneficial for imaging extrinsic indicators as they eliminate the intrinsic fluorescence background, and hence improve the image contrast.

The depth limit imposed by the signal-to-background ratio of 2PM can be overcome by 3PM. In the 1990s, several groups demonstrated the feasibility of 3PM[6–8], which was mainly used to expand the spectral coverage of the excitation source[64]. Although it was realized in these early demonstrations that 3PE significantly improves the excitation confinement[6], this advantage is largely inconsequential in imaging non-scattering samples or superficial layers of tissue. The signal-to-background ratio is mainly determined by the long-range behaviour of fluorescence generation (that is, fluorescence generation far from the focal plane), which varies as $1/z^4$ and $1/z^2$ (where z is the distance from the focal plane) for 3PE and two-photon excitation (2PE), respectively. Orders of magnitude improvement in the signal-to-background ratio can be achieved by 3PE when imaging deep into scattering tissue. Furthermore, 3PE makes a number of existing fluorophores accessible in the 1,700-nm spectral window (for example, fluorophores with one-photon absorption ~560 nm). This is particularly important as there is currently no biologically relevant fluorescent indicator for 2PE in the 1,700-nm spectral window. However, to make 3PE a practical contrast mechanism for biological imaging, a source with a high pulse energy and a low duty cycle is needed, so that an adequate signal (inversely proportional to the square of the duty cycle) can be obtained at average powers that do not cause tissue heating.

Ideal sources for deep-tissue MPM will deliver energetic (>>10 nJ) femtosecond pulses in the 1,300-nm or 1,700-nm window, with repetition rates matched to the imaging speed without causing excessive sample heating. However, the wavelength tunability of fibre lasers is limited to tens of nanometres by the gain bandwidth of the dopants, and this significantly restricts their application in biological and medical imaging.

A soliton can continuously transfer energy from a shorter to a longer wavelength via intrapulse stimulated Raman scattering; this is the soliton self-frequency shift (SSFS)[65]. Continuous tuning to longer wavelengths is achieved by simply increasing the input power[66]. In addition, soliton pulses generated through the SSFS typically have superb pulse quality and femtosecond pulse duration. The combination of fibre lasers and SSFS is ideal for MPM applications. A variety of nonlinear media have been used to demonstrate SSFS in the past, ranging from highly nonlinear PCF[67–69] to air-core photonic bandgap fibres[70]. The soliton energy is proportional to the effective mode area A_{eff}. Increasing the soliton energy by increasing the mode area is particularly effective for soliton wavelengths beyond 1,300 nm for which silica has anomalous dispersion.

The SSFS at wavelengths beyond 1,300 nm can be achieved in a variety of large-core fibres where the waveguide contribution to the dispersion is insignificant. Such design freedom allows the generation of energetic solitons whose wavelengths can be tuned over the range 1,600–2,200 nm (ref. 71). The soliton energy in a large-mode-area fibre or a photonic-crystal rod is 10–100 times higher than that in a single-mode fibre. When combined with an energetic fibre-based source at 1,550 nm, the SSFS in these structures provides a convenient mechanism for generating energetic femtosecond pulses in the 1,700-nm spectral window for deep-tissue imaging. Indeed, solitons near 1,700 nm with megawatt peak powers were obtained by using the SSFS in a photonic-crystal rod. This source was used to image neurons labelled with a red fluorescent protein in a mouse brain using 3PE (Fig. 4)[63]. Subcortical structures in an intact mouse brain were imaged *in vivo* for the first time using this approach. Although a fibre chirped-pulse-amplification system at 1,550 nm was used as the pump source, the required pulse energy is within the range of a dissipative-soliton fibre laser. Deep-tissue MPM in the long-wavelength spectral windows provides significant motivation for further development of fibre-based sources.

Fibre sources for coherent Raman microscopy

The requirement of two synchronized trains of ultrashort pulses for Raman microscopies presents a serious technical challenge. A practical light source for CRS imaging needs to satisfy the following four performance requirements: (i) it must deliver two excitation wavelengths, one of which must be tunable to enable a specific molecular vibration to be selectively excited; (ii) the two pulse trains must be synchronized and overlap temporally — the relative timing jitter should be a small fraction of the pulse width; (iii) the excitation pulse should have a narrower spectral width than the vibrational resonances — a transform-limited pulse with a duration of several picoseconds is typically ideal; (iv) both wavelengths must have sufficiently high output powers. Because of the losses of the microscope optics and overfilling of the objective lens, pulse energies of a few nanojoules are required. Therefore, an average power of at least 100 mW at a repetition rate of 10–100 MHz is desired.

The most commonly used source for CRS microscopy is a picosecond Nd-doped vanadate laser that is frequency-doubled to synchronously pump an optical parametric oscillator (OPO) based on a quadratic nonlinear crystal[72]. Commercial systems that offer excellent performance have been developed (for example, Levante Emerald™, APE GmbH), but the cost, complexity and limited potential for integrating bulk solid-state lasers have impeded the widespread application of Raman imaging in biomedical research. The need for a fibre-based source that is robust and cost-effective is even more urgent for clinical environments.

Several fibre-based sources for CRS imaging have been reported in the past few years. An early optical parametric amplifier (OPA) generated picosecond and femtosecond pulses with an all-fibre design[73]. One recent approach is based on frequency shifting the output from a picosecond Er-doped fibre laser in a nonlinear fibre and then using second-harmonic generation to reach the desired wavelengths[74]. Another uses the output from an Er-doped fibre laser to generate the higher-frequency light through second-harmonic generation and the lower-frequency light by filtering a supercontinuum[75]. These sources can be integrated, but higher output powers are desirable for many biological imaging applications.

Four-wave mixing (FWM) in a fibre (typically a dispersion-engineered PCF) is the basis of several OPAs designed for CRS imaging. FWM in the normal-dispersion regime can produce the spectrally narrow but widely spaced frequency bands desired for CRS microscopy[76]. An all-fibre OPA was successfully used to perform CARS imaging, but it generates long (~140 ps) pulses, which yield much lower peak powers than pulses from solid-state sources[77].

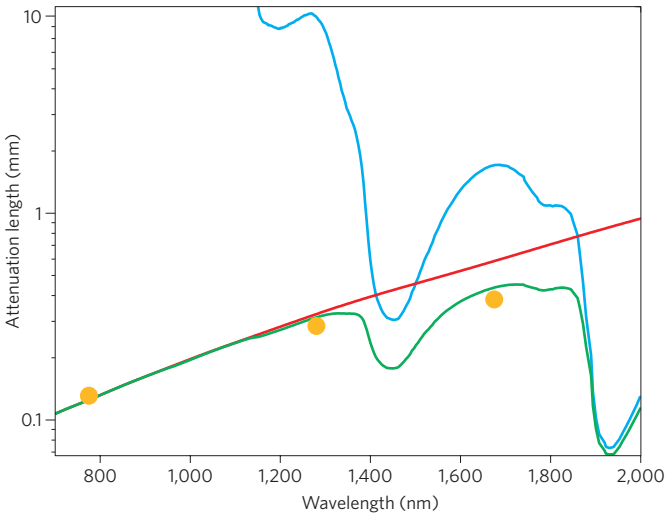

Figure 3 | Attenuation length in brain tissue as a function of wavelength. The water absorption length (blue line), the scattering length of mouse brain cortex (red line) and the effective attenuation length (green line). Note the logarithmic scale of the vertical axis. The scattering length is obtained by numerical simulation using Mie theory for a tissue-like phantom that has similar scattering properties as the cortex. The phantom contains 1-mm-diameter polystyrene beads at a concentration of 5.4×10^9 ml^{-1}. The yellow circles indicate the reported attenuation lengths for mouse cortex *in vivo* from previous studies[58,61].

Spontaneous FWM naturally produces a highly fluctuating output. Lefrancois *et al.* showed that seeding the FWM process not only reduces the fluctuations (which was well known), it also allows the generation of high-energy, transform-limited picosecond pulses by suppressing continuum generation and Raman scattering[78]. This led to the development of the first fibre source that matches the pulse parameters of the solid-state OPO[72]. An Yb-doped fibre laser drives the FWM process, which produces 3-nJ and 2-ps pulses tunable around 800 nm (Fig. 5). These pulses are combined with 1050-nm pulses from the fibre laser to excite vibrational modes between 2,650 and 3,200 cm^{-1}. High-quality CARS images (Fig. 5) of mouse ear and brain, as well as fibroblast cells, were obtained using this source.

Attention has recently turned to the development of OPOs based on FWM. A fibre OPO with a femtosecond seed laser has been demonstrated[79]. Multimodal CARS imaging was performed with this instrument, but the pulse energy was fairly low (0.1–0.5 nJ). Very recently, an OPO based on FWM at normal dispersion reached the performance levels of the corresponding OPA[78] — at least twice the peak power and three times the average power of other fibre sources — with a major reduction in intensity fluctuations[80]. This enables faster imaging with a better signal-to-background ratio. In terms of practical advantages, an OPO is more efficient than an OPA and it eliminates the need for a tunable, narrowband (and hence expensive) seed laser.

A fibre laser can be used to provide one of the two wavelengths for CRS imaging; this requires the fibre laser to be synchronized to a wavelength-tunable source. In free-space lasers or OPOs, phase-locked loops and mechanical cavity adjustments are used to dynamically match the cavity lengths for synchronization. In an all-fibre laser, it is more difficult to adjust the cavity over a macroscopic length. Thus, mode-locked fibre lasers are typically used as master clocks to which other pulsed sources are synchronized, making a fibre-based synchronized source difficult to realize.

The time-lens approach[81,82] explores a new route to generate energetic picosecond pulses in an all-fibre configuration.

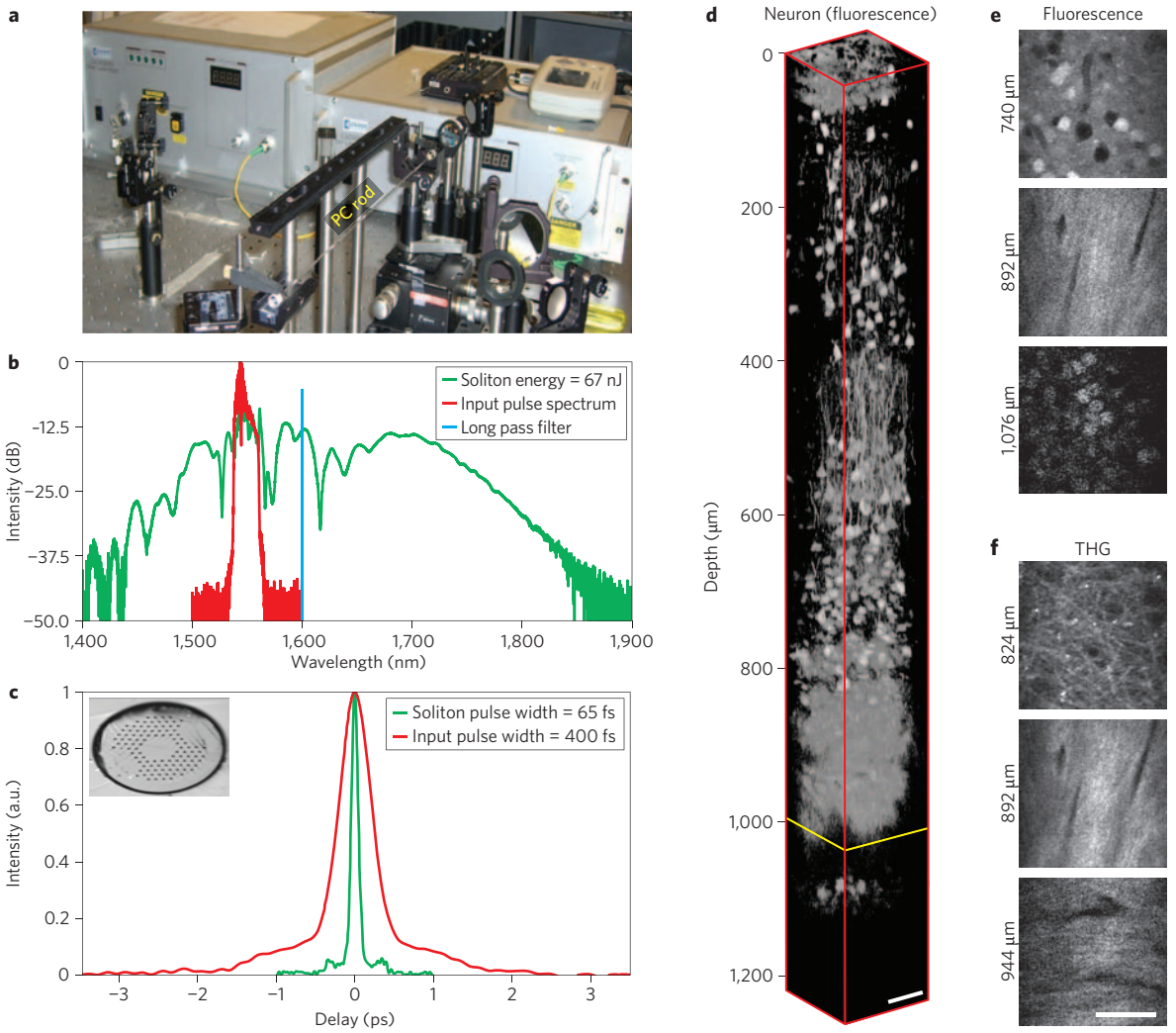

Figure 4 | SSFS in a photonic-crystal rod and *in vivo* 3PM of subcortical structures in a mouse brain. a, Experimental set-up of SSFS in a photonic-crystal rod pumped by a fibre chirped-pulse-amplification system. **b**,**c**, The measured spectrum (**b**) and the corresponding second-order autocorrelation trace (**c**) of the input pulse (red) and the 1,675-nm soliton generated in the photonic-crystal rod (green). The soliton energy, integrated from 1,617 nm, is 67 nJ. The inset in **c** shows the cross-section of the photonic-crystal rod. **d**, Three-dimensional reconstruction of *in vivo* 3PM images of mouse brain, which contains RFP-labelled pyramidal neurons. The external capsule extends from approximately 840 to 976 μm below the surface of the brain, and the stratum pyramidale extends from approximately 1,060 to 1,120 μm below the surface. **e**,**f**, Normalized *x*-*y* frames of the fluorescence (**e**) and third-harmonic generation (**f**) signals at various depths. The scale bar is 50 μm.

In contrast to mode locking, ultrafast pulses are directly 'synthesized' from continuous-wave light in this approach. By electro-optic phase modulation (that is, the time lens), a broad spectral bandwidth is generated, and this is subsequently compressed into a short pulse by dispersive elements (for example, a chirped fibre Bragg grating). Picosecond time-lens sources have been realized with telecom components[83]. Video-rate CRS imaging of mouse tissues[84] and almost shot-noise-limited stimulated Raman scattering imaging[85] have been demonstrated using time-lens sources synchronized to Ti:sapphire lasers. As the repetition rate of a time-lens source is entirely determined by an electrical drive signal, an all-fibre time-lens source can synchronize to a mode-locked laser (solid state or fibre based) at any repetition rate. In addition, electronic delay is used to adjust the relative time delay for temporal overlap of the excitation pulses, eliminating the mechanical optical delay line and its effect on spatial alignment. Unlike pulses from lasers, pulses from time-lens sources have some secondary structure in the time domain.

Summary and perspective

Recent advances in short-pulse fibre sources will impact several aspects of bioimaging. Femtosecond oscillators that can match the performance of solid-state lasers will find applications, and higher-power versions will offer some wavelength versatility through nonlinear optics. Sources in the long-wavelength excitation windows, combined with three-photon excitation, will enhance deep-tissue imaging capabilities. Coherent Raman microscopies should benefit substantially from recent developments in fibre sources of synchronized picosecond pulses with high energy.

Priorities for future development include the following.

Femtosecond sources at new wavelengths. Although 3PM at 1,700 nm has yielded record imaging depth in mouse brain, some of the most commonly used fluorophores, such as the green fluorescent protein, cannot be excited in this window. Excitation on the short-wavelength side of the water absorption, near 1,300 nm, will allow much higher excitation powers to be produced at the focus

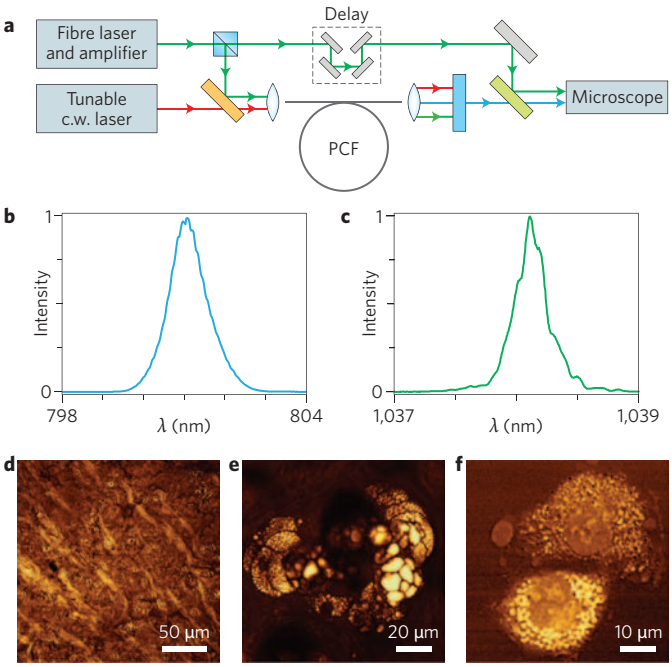

Figure 5 | Fibre source for CARS microscopy and imaging of mouse tissue. **a**, Schematic of fibre source based on FWM in PCF. c.w., continuous wave. **b**,**c**, Spectra of generated pulses. **d**–**f**, CARS images obtained using the 2,850 cm^{-1} mode of CH_2 of mouse brain (**d**), sebaceous gland at a depth of 40 μm in mouse ear (**e**) and isolated rat fibroblast cells (**f**). Figure reproduced with permission from ref. 7, © 1996 Wiley.

because of lower tissue absorption. Development of a high-energy femtosecond source in the 1,300-nm window is thus desirable. Using the SSFS to shift the output of Yb-doped sources at 1,050 nm faces major challenges. Both PCFs and air-core PBFs can provide anomalous dispersion in the range 1,050–1,300 nm. However, the soliton energy in a PCF (a fraction of 1 nJ) is nearly two orders of magnitude smaller than the desired pulse energy, whereas the bandgap of air-core PBFs is not broad enough to support the entire tuning range. HOM fibres may be an alternative for SSFS below 1,300 nm. Experiments have demonstrated that launching 1,064-nm pulses into an HOM fibre with A_{eff} = 70 $μm^2$ produces 1-nJ solitons at wavelengths up to 1,300 nm. However, it is difficult to design and fabricate HOM fibres with anomalous dispersion below 1,300 nm and a large mode area[86].

Custom pulse energies and repetition rates. The pulse energy and repetition rate of the excitation source are ultimately constrained by the fluorophore cross-section and tissue photodamage. Theory and experiment show that 2PE and 3PE cross-sections of standard dyes are on the order of 10^{-49} cm^4 s $photon^{-1}$ and 10^{-82} cm^6 s^2 $photon^{-2}$, respectively[6]. Under short-pulse excitation, fluorescence saturates at the limit of one transition per pulse per fluorophore. The pulse energies for saturation of fluorescence excitation under 2PE and 3PE are then approximately 1 nJ and 5 nJ, respectively, assuming 1700-nm excitation with 100-fs pulses and a numerical aperture of 1.0. These pulse energies are significantly below the breakdown threshold for biological tissues[87] for wavelengths greater than 1,000 nm. Thus, linear absorption (which depends on the average power) is likely to be the leading concern when imaging deep into tissue using the 1,300-nm or 1,700-nm windows. The optimum excitation source should provide pulses with approximately the saturation pulse energy at the focus for various depths in the tissue, and for average power (which depends on the repetition rate) levels that are tailored to avoid significant sample heating. It is challenging to achieve the required pulse energy (hundreds of nanojoules) and repetition rate (on the order of 1 MHz) using bulk solid-state systems (the Femtosource™ XL from Femtolasers GmbH generates femtosecond pulses with hundreds of nanojoules at a repetition rate of 5 MHz). The use of fibres will greatly simplify the long cavity lengths required for low repetition rates, and new pulse evolutions allow stable high-energy pulses to be generated.

Fibre sources for Raman microscopy. There is still no all-fibre source with intensity fluctuations that are sufficiently low to permit stimulated Raman scattering images to be recorded without balanced detection. Sources with the above-stated pulse parameters and fluctuations near the fundamental limits are needed.

All-fibre, environmentally stable sources with high performance. The best-performing devices generally include some bulk optical components, which detract from the benefits of fibre to some degree. The ideal solution would be to use completely fibre-integrated instruments made with polarization-maintaining fibre. The goal is to construct integrated instruments that do not sacrifice too much of the performance attained by lasers with bulk components. New large-mode-area chirally coupled core fibres[88] offer attractive features for this direction.

The development of these fibre-based lasers has the potential to transform nonlinear microscopy. By providing compact, robust and cost-effective excitation sources, fibre lasers will increase the adoption of nonlinear imaging techniques in the biological and biomedical communities, and accelerate their clinical translation. Furthermore, fibre-based excitation sources have the potential to provide new performance parameters that are challenging to realize using bulk solid-state systems. The needs of nonlinear microscopy provide ample motivation for continued development of short-pulse fibre sources, and in turn, new fibre sources will undoubtedly expand the boundaries of bioimaging.

Received 2 August 2013; accepted 24 September 2013; published online 20 October 2013; corrected online 28 October 2013

References

1. Denk, W., Strickler, J. H. & Webb, W. W. Two-photon laser scanning fluorescence microscopy. *Science* **248,** 73–76 (1990).
2. Yuste, R. & Denk, W. Dendritic spines as basic function units of neuronal integration. *Nature* **375,** 682–684 (1995).
3. Williams, R. M., Piston, D. W. & Webb, W. W. Two-photon molecular excitation provides intrinsic 3-dimensional resolution for laser-based microscopy and microphotochemistry. *FASEB J.* **8,** 804–813 (1994).
4. Denk, W., Piston, D. W. & Webb, W. W. in *The Handbook of Confocal Microscopy* (ed. Pawley, J. B.) 445–458 (Plenum, 1995).
5. Helmchen, F. & Denk, W. Deep tissue two-photon microscopy. *Nature Methods* **2,** 932–940 (2005).
6. Xu, C., Zipfel, W., Shear, J. B., Williams, R. M. & Webb, W. W. Multiphoton fluorescence excitation: new spectral windows for biological nonlinear microscopy. *Proc. Natl Acad. Sci. USA* **93,** 10763–10768 (1996).
7. Wokosin, D. L., Centonze, V. E., Crittenden, S. & White, J. Three-photon excitation fluorescence imaging of biological specimens using an all-solid-state laser. *Bioimaging* **4,** 208–214 (1996).
8. Hell, S. W. *et al.* Three-photon excitation in fluorescence microscopy. *J. Biomed. Opt.* **1,** 71–74 (1996).
9. Campagnola, P. J., Wei, M.-D., Lewis, A. & Loew, L. M. High-resolution nonlinear optical imaging of live cells by second harmonic generation. *Biophys. J.* **77,** 3341–3349 (1999).
10. Moreaux, L., Sandre, O. & Mertz, J. Membrane imaging by second-harmonic generation microscopy. *J. Opt. Soc. Am. B* **17,** 1685–1694 (2000).
11. Barad, Y., Eisenberg, H., Horowitz, M. & Silberberg, Y. Nonlinear laser scanning microscopy by third harmonic generation. *Appl. Phys. Lett.* **70,** 922–924 (1997).
12. Müller, M., Squier, I., Wilson, K. R. & Brakenoff, G. I. 3D microscopy of transparent objects using third-harmonic generation. *J. Microsc.* **191,** 266–274 (1998).

13. Sánchez, E. J., Novotny, L. & Xie, X. S. Near-field fluorescence microscopy based on two-photon excitation with metal tips. *Phys. Rev. Lett.* **82,** 4014–4017 (1999).
14. Jung, J. C. & Schnitzer, M. J. Multiphoton endoscopy. *Opt. Lett.* **28,** 902–904 (2003).
15. Hell, S. W. & Wichmann, J. Breaking the diffraction resolution limit by stimulated emission: stimulated-emission-depletion fluorescence microscopy. *Opt. Lett.* **19,** 780–782 (1994).
16. Shaner, N. C., Steinbach, P. A. & Tsien, R. Y. A guide to choosing fluorescent proteins. *Nature Methods* **2,** 905–909 (2005).
17. Hoover, E. E. & Squier, J. A. Advances in multiphoton microscopy technology. *Nature Photon.* **7,** 93–101 (2013).
18. Duncan, M. D., Reintjes, J. & Manuccia, T. J. Scanning coherent anti-stokes Raman microscope. *Opt. Lett.* **7,** 350–352 (1982).
19. Zumbusch, A., Holtom, G. R. & Xie, X. S. Three-dimensional vibrational imaging by coherent anti-Stokes Raman scattering. *Phys. Rev. Lett.* **82,** 4142–4145 (1999).
20. Ploetz, E., Laimgruber, S., Berner, S., Zinth, W. & Gilch, P. Femtosecond stimulated Raman microscopy. *Appl. Phys. B* **87,** 389–393 (2007).
21. Freudiger, C. W. *et al.* Label-free biomedical imaging with high sensitivity by stimulated Raman scattering microscopy. *Science* **322,** 1857–1861 (2008).
22. Spence, D. E., Kean, P. N. & Sibbett, W. 60-fsec pulse generation from a self-mode-locked Ti:sapphire laser. *Opt. Lett.* **16,** 42–44 (1991).
23. Negus, D. K., Spinelli, L., Goldblatt, N. & Feuget, G. Sub-100 fs pulse generation by Kerr lens modelocking in Ti: Al_20_3. in *Tech. Digest OSA Top. Meet. Adv. Solid State Las.* (OSA, 1991).
24. Aus der Au, J., Kopf, D., Morier-Genoud, F., Moser, M. & Keller, U. 60-fs pulses from a diode-pumped Nd:glass laser. *Opt. Lett.* **22,** 307–309 (1997).
25. Hönninger, C. *et al.* Efficient and tunable diode-pumped femtosecond Yb: glass lasers. *Opt. Lett.* **23,** 126–128 (1998).
26. Druon, F., Balembois, F. & Georges, P. Laser crystals for the production of ultrashort laser pulses. *Ann. Chim. Sci. Mat.* **28,** 47–72 (2003).
27. Seas, A., Petričević, V. & Alfano, R. R. Generation of sub-100-fs pulses from a cw mode-locked chromium-doped forsterite laser. *Opt. Lett.* **17,** 937–939 (1992).
28. Fermann, M. E., Galvanauskas, A., Sucha, G. & Harter, D. Fiber-lasers for ultrafast optics. *Appl. Phys. B* **65,** 259–275 (1997).
29. Limpert, J., Roser, F., Schreiber, T. & Tunnermann, A. High-power ultrafast fiber laser systems. *IEEE J. Sel. Top. Quant. Electron.* **12,** 233–244 (2006).
30. Ruehl, A., Wandt, D., Morgner, U. & Kracht, D. Normal dispersive ultrafast fiber oscillators. *IEEE J. Sel. Top. Quant. Electron.* **15,** 170–181 (2009).
31. Fermann, M. & Hartl, I. Ultrafast fiber laser technology. *IEEE J. Sel. Top. Quant. Electron.* **15,** 191–206 (2009).
32. Valdmanis, J. A., Fork, R. L. & Gordon, J. P. Generation of optical pulses as short as 27 femtoseconds directly from a laser balancing self-phase modulation, group-velocity dispersion, saturable absorption, and saturable gain. *Opt. Lett.* **10,** 131–133 (1985).
33. Tamura, K., Ippen, E. P., Haus, H. A. & Nelson, L. E. 77-fs pulse generation from a stretched-pulse mode-locked all-fiber ring laser. *Opt. Lett.* **18,** 1080–1082 (1993).
34. Ober, M. H., Hofer, M. & Fermann, M. E. 42-fs pulse generation from a mode-locked fiber laser started with a moving mirror. *Opt. Lett.* **18,** 367–369 (1993).
35. Chong, A., Buckley, J., Renninger, W. & Wise, F. All-normal-dispersion femtosecond fiber laser. *Opt. Express* **14,** 10095–10100 (2006).
36. Renninger, W. H., Chong, A. & Wise, F. W. Dissipative solitons in normal-dispersion fiber lasers. *Phys. Rev. A* **77,** 023814 (2008).
37. Zhao, L. M., Tang, D. Y. & Wu, J. Gain-guided soliton in a positive group-dispersion fiber laser. *Opt. Lett.* **31,** 1788–1790 (2006).
38. Grelu, P. & Akhmediev, N. Dissipative solitons for mode-locked lasers. *Nature Photon.* **6,** 84–92 (2012).
39. Kieu, K., Renninger, W. H., Chong, A. & Wise, F. W. Sub-100-fs pulses at watt-level powers from a dissipative-soliton fiber laser. *Opt. Lett.* **34,** 593–595 (2009).
40. Chichkov, N. B. *et al.* Pulse duration and energy scaling of femtosecond all-normal dispersion fiber oscillators. *Opt. Express* **20,** 3844–3852 (2012).
41. Chong, A., Renninger, W. H. & Wise, F. W. Properties of normal-dispersion femtosecond fiber lasers. *J. Opt. Soc. Am. B* **25,** 140–148 (2008).
42. Renninger, W. H., Chong, A. & Wise, F. W. Self-similar pulse evolution in an all-normal-dispersion laser. *Phys. Rev. A* **82,** 021805(R) (2010).
43. Wise, F. W. Femtosecond fiber lasers based on dissipative processes for nonlinear microscopy. *IEEE J. Sel. Top. Quant. Electron.* **18,** 1412–1421 (2012).
44. Oktem, B., Ülgüdür, C. & Ilday, F. Ö. Soliton–similariton fibre laser. *Nature Photon.* **4,** 307–311 (2010).
45. Liu, G., Kieu, K., Wise, F. W. & Chen, Z. Multiphoton microscopy system with a compact fiber-based femtosecond-pulse laser and handheld probe. *J. Biophotonics* **4,** 34–39 (2011).
46. Galvanauskas, A. Mode-scalable fiber-based chirped pulse amplification systems. *IEEE J. Select Top. Quant. Electron* **7,** 504–517 (2001).
47. Lefrançois, S., Kieu, K., Deng, Y., Kafka, J. D. & Wise, F. W. Scaling of dissipative soliton fiber lasers to megawatt peak powers by use of large-area photonic-crystal fiber. *Opt. Lett.* **35,** 1569–1571 (2010).
48. Baumgartl, M., Lecaplain, C., Hideur, A., Limpert, J. & Tunnerman, A. 66 W average power from a microjoule-class sub-100 fs fiber oscillator. *Opt. Lett.* **37,** 1640–1642 (2012).
49. Ramachandran, S. *et al.* Light propagation with ultralarge modal areas in optical fibers. *Opt. Lett.* **31,** 1797–1799 (2006).
50. Nicholson, J. W. *et al.* Nanosecond pulse amplification in a 6000 μm^2 effective area higher-order mode erbium-doped fiber amplifier. Paper JTh1I.2 in *Proc. Conf. Lasers Electro Optics* (OSA, 2012).
51. Svoboda, K., Tank, D. W. & Denk, W. Direct measurement of coupling between dendritic spines and shafts. *Science* **272,** 716–719 (1996).
52. Mostany, R. & Portera-Cailliau, C. Absence of large-scale dendritic plasticity of layer 5 pyramidal neurons in peri-infarct cortex. *J. Neuroscience* **31,** 1734–1738 (2011).
53. Squirrell, J. M., Wokosin, D. L., White, J. G. & Bavister, B. D. Long-term two-photon fluorescence imaging of mammalian embryo without compromising viability. *Nature Biotechnol.* **17,** 763–767 (1999).
54. Zipfel, W. R. *et al.* Live tissue intrinsic emission microscopy using multiphoton-excited native fluorescence and second harmonic generation. *Proc. Natl Acad. Sci. USA* **100,** 7075–7080 (2003).
55. So, P. T. C., Dong, C. Y., Masters, B. R. & Berland, K. M. Two-photon excitation fluorescence microscopy. *Annu. Rev. Biomed. Eng.* **2,** 399–429 (2000).
56. Centonze, V. E. & White, J. G. Multiphoton excitation provides optical sections from deeper within scattering specimens than confocal imaging. *Biophys. J.* **75,** 2015–2024 (1998).
57. Theer, P., Hasan, M. T. & Denk, W. Two-photon imaging to a depth of 1000 µm in living brains by use of a Ti:Al_2O_3 regenerative amplifier. *Opt. Lett.* **28,** 1022–1024 (2003).
58. Leray, A., Odin, C., Huguet, E., Amblard, F. & Le Grand, Y. Spatially distributed two-photon excitation fluorescence in scattering media: experiments and time-resolved Monte Carlo simulations. *Opt. Commun.* **272,** 269–278 (2007).
59. Kobat, D., Horton, N. G. & Xu, C. *In vivo* two-photon microscopy to 1.6-mm depth in mouse cortex. *J. Biomed. Opt.* **16,** 106014 (2011).
60. Kobat, D. *et al.* Deep tissue multiphoton microscopy using longer wavelength excitation. *Opt. Express* **17,** 13354–13364 (2009).
61. Balu, M. *et al.* Effect of excitation wavelength on penetration depth in nonlinear optical microscopy of turbid media. *J. Biomed. Opt.* **14,** 010508 (2009).
62. Andresen, V. *et al.* Infrared multiphoton microscopy: subcellular resolved deep tissue imaging. *Curr. Opin. Biotechnol.* **20,** 54–62 (2009).
63. Horton, N. G. *et al. In vivo* three-photon microscopy of subcortical structures of an intact mouse brain. *Nature Photon* **7,** 205–209 (2009).
64. Maiti, S., Shear, J. B., Williams, R. M., Zipfel, W. R. & Webb, W. W. Measuring serotonin distribution in live cells with three-photon excitation. *Science* **275,** 530–532 (1997).
65. Gordon, J. P. Theory of the soliton self-frequency shift. *Opt. Lett.* **11,** 662–664 (1986).
66. Zysset, B., Beaud, P. & Hodel, W. Generation of optical solitons in the wavelength region 1.37–149 µm. *Appl. Phys. Lett.* **50,** 1027–1029 (1987).
67. Liu, X. *et al.* Soliton self-frequency shift in a short tapered air-silica microstructure fiber. *Opt. Lett.* **26,** 358–360 (2001).
68. Knight, J. C., Broeng, J., Birks, T. A. & Russell, P. St. J. Photonic band gap guidance in optical fibers. *Science* **282,** 1476–1478 (1998).
69. Unruh, J. R. Two-photon microscopy with wavelength switchable fiber laser excitation. *Opt. Express* **14,** 9825–9831 (2006).
70. Ouzounov, D. G. Generation of megawatt optical solitons in hollow-core photonic band-gap fibers. *Science* **301,** 1702–1704 (2003).
71. Wang, K. & Xu, C. Tunable high-energy soliton pulse generation from a large-mode-area fiber and its application to third harmonic generation microscopy. *Appl. Phys. Lett.* **99,** 071112 (2011).
72. Ganikhanov, F. Broadly tunable dual-wavelength light source for coherent anti-Stokes Raman scattering microscopy. *Opt. Lett.* **31,** 1292–1294 (2006).
73. Andresen, E. R., Nielsen, C. K., Thøgersen, J. & Keiding, S. R. Fiber laser-based light source for coherent anti-Stokes Raman scattering microspectroscopy. *Opt. Express* **15,** 4848–4856 (2007).
74. Krauss, G. *et al.* Compact coherent anti-Stokes Raman scattering microscope based on a picosecond two-color Er:fiber laser system. *Opt. Lett.* **34,** 2847–2849 (2009).
75. Kieu, K. & Peyghambarian, N. Synchronized picosecond pulses at two different wavelengths from a compact fiber laser source for Raman microscopy. Paper 790310 in *SPIE BiOS* (SPIE, 2011).

76. Mosley, P. J., Bateman, S. A., Lavoute, L. & Wadsworth, W. J. Low-noise, high-brightness, tunable source of picosecond pulsed light in the near-infrared and visible. *Opt. Express* **19,** 25337–25345 (2011).
77. Baumgartl, M. *et al.* Alignment-free, all-spliced fiber laser source for CARS microscopy based on four-wave-mixing. *Opt. Express* **20,** 21010–21018 (2012).
78. Lefrancois, S. *et al.* Fiber four-wave mixing source for coherent anti-Stokes Raman scattering microscopy. *Opt. Lett.* **37,** 1652–1654 (2012).
79. Zhai, Y.-H. *et al.* Multimodal coherent anti-Stokes Raman spectroscopic imaging with a fiber optical parametric oscillator. *Appl. Phys. Lett.* **98,** 191106 (2011).
80. Lamb, E. *et al.* Fiber optical parametric oscillator for coherent anti-Stokes Raman scattering microscopy *Opt. Lett.* **38,** 4154–4157 (2013).
81. Godil, A. A., Auld, B. A. & Bloom, D. M. Picosecond time-lenses. *IEEE J. Quantum Electron.* **30,** 827–837 (1994).
82. Kolner, B. H. Space-time duality and the theory of temporal imaging. *IEEE J. Quantum Electron.* **30,** 1951–1963 (1994).
83. Van Howe, J., Hansryd, J. & Xu, C. Multiwavelength pulse generator using time-lens compression. *Opt. Lett.* **29,** 1470–1472 (2004).
84. Wang, K. *et al.* Synchronized time-lens source for coherent Raman scattering microscopy. *Opt. Exp.* **23,** 24019–24024 (2010).
85. Wang, K. *et al.* Time-lens based hyperspectral stimulated Raman scattering imaging and quantitative spectral analysis. *J. Biophotonics* **6,** 815–820 (2013).
86. Pedersen, M. E. V. *et al.* Higher-order-mode fiber optimized for energetic soliton propagation. *Opt. Lett.* **37,** 3459–3461 (2012).
87. Olivié, G. *et al.* Wavelength dependence of femtosecond laser ablation threshold of corneal stroma. *Opt. Express* **16,** 4121–4129 (2008).
88. Liu, C.-H. Paper ME2 Effectively single-mode chirally-coupled core fiber. Paper ME2 in *Advanced Solid-State Photonics* (OSA, 2007).

Acknowledgements

Portions of this work were supported by the National Institutes of Health (EB002019, R01CA133148, R01EB014873 and R21RR032392) and the National Science Foundation (ECCS-0901323, BIS-0967949).

Additional information

Reprints and permissions information is available at www.nature.com/reprints. Correspondence and requests for materials should be addressed to C.X. and F.W.W.

Competing financial interests

F. W. Wise is a named inventor on US patent US 8,416,817 B2 (publication date 04.09.2008, filing date 18.09.2007) and Chinese patent number 200780042670.8, which are related to the dissipative-soliton laser described in this Review Article. European patent application number 7873804.4 has been filed on the same subject. Wise has also submitted a patent application relating to picosecond-pulse sources for coherent anti-Stokes Raman microscopy (international patent PCT/US/2012/058817 (publication date 11.04.2013, filing date 04.10.2011).

CORRIGENDUM

Recent advances in fibre lasers for nonlinear microscopy

C. Xu & F. W. Wise

Nature Photon. **7,** 875–882 (2013); published online 20 October 2013; corrected after print 28 October 2013.

In the version of this Review Article originally published online and in print, no competing financial interests were declared. However, the authors wish to acknowledge relevant patents. The competing financial interests statement in the HTML and PDF versions of the Review Article has been modified to that shown below:

F. W. Wise is a named inventor on US patent US 8,416,817 B2 (publication date 04.09.2008, filing date 18.09.2007) and Chinese patent number 200780042670.8, which are related to the dissipative-soliton laser described in this Review Article. European patent application number 7873804.4 has been filed on the same subject. Wise has also submitted a patent application relating to picosecond-pulse sources for coherent anti-Stokes Raman microscopy (international patent PCT/US/2012/058817 (publication date 11.04.2013, filing date 04.10.2011).